NASA Technical Paper 1205

Theoretical Flow Characteristics of Inlets for Tilting-Nacelle VTOL Aircraft

Michael A. Boles, Roger W. Luidens,
and Norbert O. Stockman

APRIL 1978

NASA

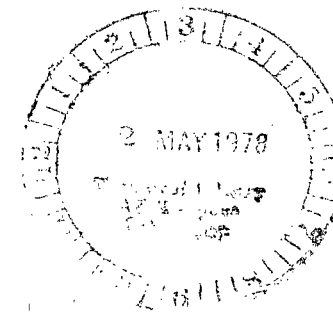

NASA Technical Paper 1205

Theoretical Flow Characteristics of Inlets for Tilting-Nacelle VTOL Aircraft

Michael A. Boles, Roger W. Luidens,
and Norbert O. Stockman
Lewis Research Center
Cleveland, Ohio

National Aeronautics
and Space Administration

**Scientific and Technical
Information Office**

1978

THEORETICAL FLOW CHARACTERISTICS OF INLETS FOR TILTING-NACELLE VTOL AIRCRAFT

by Michael A. Boles,* Roger W. Luidens, and Norbert O. Stockman

Lewis Research Center

SUMMARY

The results of a theoretical investigation of geometric variables for lift-cruise-fan tilting-nacelle inlets operating at high incidence angles are presented. These geometric variables are investigated for their effects on surface static-to-free-stream-total-pressure ratio and the separation parameters of maximum-to-diffuser-exit-surface-velocity ratio and maximum surface Mach number for low-speed (takeoff and landing) operation. The geometric parameters varied were the internal-lip contraction ratio, external-forebody-to-diffuser-exit-diameter ratio, external-forebody length-to-diameter ratio (these latter two were established by drag-divergence Mach number specification), and internal-lip major-to-minor-axis ratio.

Low-speed results were obtained at three levels of free-stream Mach number to 0.18, three values of one-dimensional throat Mach number, and incidence angles from 0 to 120°. The results indicate that of the geometric variables studied, contraction ratio had the largest effect on the separation parameters.

The effects of inlet contraction ratio and drag divergence Mach number on maximum external surface Mach numbers and maximum-to-highlight-diameter ratio are illustrated at cruise Mach number 0.7 to 0.8.

INTRODUCTION

Lift-cruise fans contained in tilting nacelles are being considered for a VTOL aircraft. The inlets of these nacelles must operate over a wide range of incidence angles,

*Head of the Division of Engineering, Indiana Institute of Technology, Fort Wayne, Indiana; Summer Faculty Fellow at the Lewis Research Center in 1975 and 1976.

flight speeds, and throttle settings during takeoff and landing. The inlet design is one of the major concerns for the tilting lift-cruise fan because at large incidence angles the inlet internal flow may separate. The fan-face flow distortion due to separation will cause increased fan blade stress and may cause core-compressor stall. Separation-free internal flow is largely a function of the internal-lip geometry. The external-lip geometry must be compatible with the internal geometry and must be designed to avoid drag rise at cruise. The overall inlet should be as short and as small in diameter as possible to minimize friction drag and weight. Thus, the overall lift-cruise inlet design becomes a compromise between the internal and external lip shapes for best low-speed and cruise performances.

Experimental and theoretical studies (refs. 1 to 8) have been conducted to determine the effects of geometry and flow conditions on the performance of engine nacelle inlets for short-haul aircraft, which will operate at similar, but somewhat less difficult, flow conditions. The experimental performance of engine inlets for short-haul aircraft are reported in references 1 to 5. Theoretical studies using potential flow and boundary layer analysis are presented in references 3 to 8.

This report presents the results of a theoretical study to investigate the design of inlets for tilt nacelle VTOL aircraft. Based on probable flight paths for a tilt-nacelle VTOL aircraft (fig. 1), the following flow conditions were selected for analysis: incidence angles up to 90° for free-stream Mach numbers of 0.12 and 0.18, and an incidence angle of 120° at free-stream Mach number of 0.06, and a range of throat Mach numbers from 0.25 to 0.70. Cruise flight Mach numbers from 0.70 to 0.80 are also considered. The geometric parameters varied were the internal lip contraction ratio, internal lip major-to-minor-axis ratio, nacelle-maximum-diameter-to-diffuser-exit-diameter ratio, and external-forebody-length-to-maximum-diameter ratio.

These flow and geometric variables are investigated for their effects on the following dependent quantities: the surface-static-pressure distribution, peak surface Mach number, and diffusion ratio (ratio of maximum surface velocity to diffuser exit velocity). The last two parameters have been shown (ref. 9) to be good indications of whether the inlet flow is attached or separated. Experimental limits on these parameters (determined in ref. 9 for three STOL model inlets) will be applied to the theoretical results for the VTOL inlets of the present study.

SYMBOLS

A area

a major axis of internal lip (fig. 2)

b minor axis of internal lip (fig. 2)

D diameter

L length (fig. 2)

M Mach number

P_s static pressure

P_{tot} total pressure

S local surface distance from inlet highlight (fig. 2)

S_{ref} surface distance from inlet highlight to diffuser exit (fig. 2)

V velocity

$\bar{x}$ external forebody length (fig. 2)

x axial distance from inlet highlight

$\bar{y}$ external forebody thickness (fig. 2)

y radial distance from inlet highlight

α incidence angle of inlet, angle between free-stream velocity and inlet axis (fig. 2)

Subscripts:

c centerbody

d diffuser

dd drag divergence

e exit or tip

ext external

h highlight

max maximum

t throat

0 free stream

DESCRIPTION OF GEOMETRIES

The nomenclature used and the principal inlet geometric variables are illustrated in figure 2. For the inlets investigated the internal-lip geometry and external-forebody geometry were varied, and the diffuser geometry and the centerbody were fixed (table I). The internal-lip profile was an ellipse and was characterized by the inlet contraction ratio, defined as the ratio of the highlight area to throat area $(D_h/D_t)^2$, and the major-to-minor-axis ratio a/b. Inlet contraction ratios ranged from 1.46 to 2.8

(fig. 3(a)). The value of a/b was 2.0 for all cases, except the 1.65 contraction ratio inlet (fig. 3(b)) for which a/b values of 1.5 and 2.0 were investigated. The external-forebody profile was a bisuper-ellipse curve of the form (ref. 8).

$$\left(\frac{x}{\bar{x}}\right)^{1.77} + \left(\frac{y}{\bar{y}}\right)^{2.25} = 1 \tag{1}$$

The external-forebody geometric parameters were the ratio of external-forebody length to maximum diameter $\bar{x}/D_{max}$ and the ratio of highlight to maximum diameter D_h/D_{max}. The values of these parameters were selected for prescribed values of drag-divergence Mach number (ref. 3). The effect of drag-divergence Mach number for inlets with a specified internal geometry is shown in figure 3(c). The values of contraction ratios, lip major-to-minor axis ratios, and drag-divergence Mach numbers chosen for this study are presented in table II.

METHOD OF SOLUTION

The theoretical potential flow at the various operating conditions for the inlets was obtained using the calculation procedures for engine inlets presented in reference 10. Briefly, the basic elements of the potential-flow-computer-program system are (1) a program for geometry definition, (2) an incompressible potential-flow calculation program, and (3) a program to combine basic potential flow solutions into solutions of interest (having specified values of free-stream velocity, incidence angle, and inlet mass flow) and also to correct the results for compressibility effects and local supersonic Mach number effects.

The potential-flow calculations were used to obtain surface-pressure distributions, peak Mach numbers and diffusion ratios for the several inlet geometries and various flow conditions. All potential-flow results shown are for the windward (see fig. 2) side of the inlet since the most severe flow conditions occur at this position.

SEPARATION PARAMETERS

A review of experimental results reveals that two separation parameters are important (ref. 9): the diffusion ratio (ratio of maximum surface velocity to diffuser exit velocity) and the peak Mach number (maximum surface Mach number).

Results from the inlet tests of reference 2 were used in reference 9 to identify the range of these parameters at the onset of large-scale flow separation. The inlets used

in reference 9 were STOL model inlets, similar to the inlets (table II) of this report, and have contraction ratios of 1.37, 1.46, and 1.56. Experimental flow-separation data from those inlets are shown in figure 4. There, the peak Mach number and the diffusion ratio at the onset of flow separation appear as functions of the ratio of one-dimensional throat Mach number to free-stream Mach number M_t/M_0.

Each data point in figure 4 is a separation limit for its flow condition. In figure 4(a) peak Mach number curves increase with increasing M_t/M_0 up to a limit. These peak Mach number limits form a band in the range of 1.4 to 1.6. Points lying outside this band are diffusion limited (fig. 4(b)). These diffusion limits increase somewhat with increasing M_t/M_0 but still lie in a band in the range of 2.4 to 2.9. Here, the data points that fell outside the peak Mach number limit band fall within the diffusion limit band.

In summary, at lower throat Mach numbers the separation-free flow appears to be diffusion-ratio limited, and at higher throat Mach numbers the separation-free flow appears to be peak-Mach-number limited.

RESULTS AND DISCUSSION

The dependent parameters discussed are inlet surface pressure ratio, peak surface Mach number, and diffusion velocity ratio. The independent variables are contraction ratio, lip major-to-minor-axis ratio, external-forebody geometry, free-stream Mach number, incidence angle, and one-dimensional throat Mach number. All data are presented for the windward side of the inlet since the most severe flow conditions occur at this position.

Low Speed Flow Conditions

The inlets considered in this section all have an internal lip major-to-minor-axis ratio of 2.0 and a drag-divergence Mach number of 0.77 (table II and fig. 3).

Effect of incidence angles to 90°. - The results in this section are for a one-dimensional throat Mach number of 0.70 and a free-stream Mach number of 0.12. Figure 5 shows the surface pressures as a function of dimensionless distance from highlight for several incidence angles and several contraction ratios. In general, the surface lip (highlight to throat) pressures increase with increasing contraction ratio and decrease with increasing incidence angle. For small incidence angles (α of 0° and 30°) the minimum static pressure occurs near the throat for all contraction ratios; thus, for these angles very little diffusion takes place on the inlet lip. For larger incidence angles (α's of 60° and 90°) the minimum static pressure occurs at the highlight region for

contraction ratios of 1.46 and 1.65, and there can be significant diffusion on the lip; but at contraction ratios of 2.2 and 2.8 the minimum static pressure remains near the throat.

The key dependent parameters, diffusion ratio V_{max}/V_{de} and the peak Mach number M_{max}, are plotted in figure 6 as functions of contraction ratio. The curves show a diminishing advantage (i.e., reduction of peak Mach number and diffusion ratio) of increasing contraction ratio above about 2.0 for a given α. The same dependent parameters are cross-plotted in figure 7 as functions of incidence angle. There it can be seen that incidence has relatively little effect for contraction ratios of 2.2 or greater.

Effect of throat Mach number and free-stream Mach number. - The effects of decreasing throat Mach number at two free-stream Mach numbers are presented here. Figure 8 illustrates the effect of decreasing M_t from 0.70 to 0.25 on the surface static-pressure distribution for contraction ratios of 1.46 to 2.8, an a/b of 2.0, and a M_0 of 0.12 at an incidence angle of 90^o. This figure indicates that the flow becomes locally supersonic for all flow conditions for the 1.46 and 1.65 contraction ratios but remains subsonic for the 2.20 and 2.80 contraction ratios. Figure 8 also shows that decreasing the throat Mach number increases the initial diffusion rate (pressure gradient after minimum pressure point) and the diffusion ratio but lowers the peak Mach number for all the contraction ratios.

Figure 9 shows the same relationship as figure 8 at an M_0 of 0.18. In all cases increasing M_0 (compare figs. 8 and 9) lowers the static pressure near the highlight, thus producing a greater overall diffusion requirement (since for a given M_t the pressure ratio at the diffuser exit is independent of M_0).

The effects of varying throat Mach number at $M_0 = 0.12$ on V_{max}/V_{de} and M_{max} are shown in figure 10. Decreasing the throat Mach number tends to increase V_{max}/V_{de} (fig. 10(a)) for all contraction ratios. The trend for M_{max} (fig. 10(b)) is to increase with increasing throat Mach number. The effect of increasing contraction ratio is to decrease both V_{max}/V_{de} and M_{max} at a given throat Mach number.

Figure 11 shows similar plots for $M_0 = 0.18$. The effect of the increased free-stream Mach number is to increase the overall level of the diffusion ratio and the peak Mach number.

Incidence angles up to 120^o may be experienced during low-speed flare to landing conditions where fan thrust is used to decelerate the VTOL aircraft. (See fig. 1.) Figure 12 presents the effect of decreasing M_t from 0.70 to 0.25 on the surface-static-pressure distribution for contraction ratios of 1.46 to 2.80, an a/b of 2.0, a free-stream Mach number of 0.06, and an incidence angle of 120^o.

This figure shows that at $M_t = 0.70$ the minimum static-pressure decreases and its location moves from the throat region to the highlight with decreasing contraction ratio. At a contraction ratio of 1.65 the flow becomes supersonic, and the pressure ratio becomes relatively flat between highlight and throat. At $M_t = 0.25$ (fig. 12(b)) the

pressure distribution appears less severe than at $M_t = 0.70$; however, figure 13 indicates that this is not necessarily the case. Figure 13 shows V_{max}/V_{de}, and M_{max} plotted as functions of contraction ratio for $M_t = 0.70$ and 0.25. This figure illustrates the increase in V_{max}/V_{de} as M_t is decreased from 0.70 to 0.25. At these low-speed operating conditions V_{max}/V_{de} is the separation controlling parameter (fig. 4).

Effects of incidence angle and contraction ratio at low speed. - Figure 14 presents a summary of the effects of contraction ratio and incidence angle for $M_t = 0.25$ and 0.70 and for $M_0 = 0.12$ and 0.18. The figure shows that increasing contraction ratio reduces V_{max}/V_{de} and M_{max} at all incidence angles and also reduces the rate of change of these parameters with incidence angle.

Generalization of flow effects. - An attempt to eliminate M_0 as an independent variable is shown in figure 15. Here, V_{max}/V_{de} and the new ratio M_{max}/M_0 are presented as functions of M_t/M_0 for α's of 60° and 90°. This use of M_t/M_0 as the dependent variable does a reasonably good job of collapsing the data for the two values of M_0 (0.12 and 0.18) for all contraction ratios and at the two incidence angles (60° and 90°) presented here. This result is believed to be valid for other incidence angles although insufficient data were generated to substantiate this. Thus, from these curves, the values of V_{max}/V_{de} and M_{max} can be estimated for other specified values of M_t, M_0, and contraction ratios for these inlets.

In figure 16 the experimental diffusion-limit band (fig. 4) has been superimposed on the plots of the diffusion ratio of figure 15. Regions of expected separated and attached flow are shown. It can be seen that low M_t conditions are likely to lie in the diffusion-limited separation region. This figure also shows that movement from the diffusion-limited separated-flow region to the attached-flow region at a given flow condition can be accomplished by increasing the contraction ratio.

The experimental peak Mach number limit band of figure 4 has been superimposed on the peak Mach number plots of figure 17 for $M_0 = 0.12$ and 0.18 and $\alpha = 60^\circ$ and 90°. Regions of expected separated and attached flow are noted. High throat Mach number flow conditions are more likely to lie in the maximum-surface-Mach-number-limited separated-flow region. For given flow conditions increasing contraction ratio a sufficient amount moves the maximum surface Mach number into the attached region.

Effect of Lip Major-to-Minor-Axis Ratio and External Forebody Shape at Low Speeds

The previous sections have been concerned with the effect of contraction ratios and low-speed flow conditions for fixed values of internal lip major-to-minor-axis ratio and external-forebody shape. In this section the effects of lip major-to-minor-axis ratio and external-forebody shape are investigated.

Effect of internal lip major to minor axis ratio. - The effect of major-to-minor internal-lip axis ratio, a/b, on the surface-static-pressure distribution for the 1.65 contraction-ratio inlet having an external forebody designed for a 0.77 drag-divergence Mach number is presented in figure 18. The flow conditions are for $\alpha = 90^{\circ}$, $M_t = 0.25$ and 0.70, and $M_0 = 0.18$. The lip geometries corresponding to the two a/b ratios of 1.5 and 2.0 are illustrated in figure 3(b). Since the pressure ratio varies inversely with curvature, the significant variation for the two a/b ratios in the shape of the surface pressure ratio curves between the highlight and throat locations can be partly explained by the differences in curvature distribution for these inlets. The inlet with an a/b of 1.5 has a lower curvature (thus larger pressure ratio) at the highlight but a larger curvature (thus smaller pressure ratio) at the throat.

Figure 19 illustrates the effects of a/b and M_0 on the variations of the separation parameters V_{max}/V_{de} and M_{max} with incidence angle for the 1.65-contraction-ratio inlet at two values of M_t. Figure 19(a) shows that at $\alpha < 90^{\circ}$ the 1.5-a/b inlet clearly yields higher diffusion ratios and maximum surface Mach numbers than the 2.0-a/b inlet. At $\alpha = 90^{\circ}$ the 1.5-a/b inlet has a lower peak Mach number than the 2.0-a/b inlet; however, this value is still within the peak Mach number limit band of figure 4.

At a low throat Mach number of 0.25 (fig. 19(b)) the 1.5-a/b inlet gives an advantage in reducing both the overall velocity ratio and maximum surface Mach number at $\alpha = 60^{\circ}$ and 90° and $M_0 = 0.12$ and 0.18.

Effect of external forebody shape. - The effect of drag-divergence Mach number on external forebody geometry is shown in figure 3(c) for the inlets with contraction ratios of 1.46 and 2.8. The effect of external forebody design for the 1.65 contraction ratio and 2.0-a/b inlet on pressure-ratio distribution is shown in figure 20. The primary variation with external-forebody design through the specified drag-divergence Mach number is in the region of the minimum static pressure ratio near the highlight. For $M_t = 0.25$ and 0.70, the minimum pressure ratio increases with increasing drag-divergence Mach number, and the local adverse pressure gradient becomes less severe for the inlets in this report. This result is partially explained by the fact that lower-drag-divergence-Mach-number inlets have larger curvature at the highlight. The effect of drag-divergence Mach number variation for an a/b of 2.0 and all contraction ratios studied in this report is summarized in figure 21 for $M_t = 0.25$ and 0.70, $M_0 = 0.18$, and $\alpha = 90^{\circ}$. Considering the increase in nacelle size (table II and fig. 3(c)) with drag-divergence Mach number, this figure shows little overall effect of drag-divergence Mach number on the separation parameters studied at low-speed conditions.

Cruise Flow Conditions

For each of the inlets of table II a potential flow analysis at the cruise Mach number ($M_0 = M_{dd} - 0.02$) was performed. Figure 22(a) shows the variation of maximum external surface Mach number with cruise Mach number for these contraction ratios. This figure shows the maximum surface Mach number on the external forebody to be only a weak function of the cruise Mach number corresponding to the design drag-divergence Mach number.

Figure 22(b) illustrates the effect of cruise at off-design conditions for the nominal 0.77 drag-divergence Mach number forebody. There is a significant increase in the external-forebody peak Mach number for cruise at higher than design cruise Mach number and a corresponding decrease for cruise at lower than design cruise Mach number. These results, along with those shown in figure 21, indicate the maximum Mach number on both the external and internal surfaces and the diffusion ratio can be decreased for all contraction ratios by designing the external forebody for higher drag divergence; however, this would require an increase in the nacelle maximum diameter and thickness.

Figure 23 presents the effect of contraction ratio and drag-divergence Mach number on the relation between maximum-to-diffuser-exit-diameter ratio and design cruise Mach number. The increase in the diameter ratio is greater than a predicted increase that had been based on contraction ratio increases alone. Significant increases in the diameter ratio occur at the 2.8 contraction ratio as drag divergence is increased as design cruise Mach number increases. Thus, the advantages of larger contraction ratio and high-drag-divergence Mach number bring with them the penalties of increased maximum nacelle diameter, and thus, higher nacelle drag and weight.

Some of the penalty resulting from the low-speed contraction ratio requirement can be eliminated by going to an asymmetric inlet with circumferentially varying contraction ratio. Since the low-speed problem area is on the windward lip, only this portion of the inlet need have the large contraction ratio; the contraction ratio on the leeward side can be smaller for more efficient cruise. Figure 24 gives an example of what might be accomplished by such an approach.

A typical large contraction ratio symmetrical inlet is illustrated in figure 24(a); figure 24(b) shows an asymmetric inlet with a 1.3 contraction ratio on the leeward side and a large contraction ratio on the windward side. A comparison of the frontal area ratio (an indicator of drag and weight) for the symmetric and asymmetric inlets is shown in figure 24(c). The asymmetric frontal area is based on a configuration having a 1.3 contraction at the leeward meridian and the large contraction ratio (which is varied as a parameter on the figure) at the windward with a smooth variation in between. It can be seen that for large contraction ratios the asymmetric inlet can significantly reduce the frontal area compared with the symmetric inlet.

SUMMARY OF RESULTS

The effect of forebody design on the aerodynamic performance was investigated for inlets of tilting-nacelle VTOL aircraft. The major geometric variables investigated were internal-lip contraction ratio, internal-lip major-to-minor-axis ratio and external-forebody parameters based on a specified drag divergence Mach number. Some specific results of this study are as follows:

1. For given flow conditions increasing contraction ratio a sufficient amount results in diffusion velocity ratios and surface Mach numbers that are less than the separation-limited values. However, increasing contraction ratio above about 2.0 results in lower reductions in the separation parameters. Furthermore, as contraction ratio is increased, the designer is faced with larger nacelle maximum diameters, which results in larger nacelle drag and weight.

2. Reducing the internal lip major-to-minor-axis ratio from 2.0 to 1.5 improves separation-free performance at higher angles of attack at sufficiently large ratio of free-stream to throat Mach number.

3. External forebodies designed for increased drag divergence Mach number resulted in increased nacelle maximum diameter and, thus, higher nacelle drag and weight, while the low-speed separation parameters were only slightly decreased.

4. The optimum forebody for the tilting nacelle may be an asymmetric inlet having a large contraction-ratio lip on the windward side where the most severe flow conditions exist and a smaller contraction-ratio lip at the leeward side where less severe flow conditions exist.

Lewis Research Center,
National Aeronautics and Space Administration,
Cleveland, Ohio, January 20, 1978,
505-05.

REFERENCES

1. Jakubowski, A. K.; and Luidens, R. W.: Internal Cowl-Separation at High Incidence Angles. AIAA Paper 75-64, Jan. 1975.

2. Miller, Brent A.; Dastoli, Benjamin J.; and Wesoky, Howard L.: Effect of Entry-Lip Design on Aerodynamics and Acoustics of High-Throat-Mach-Number Inlets for the Quiet, Clean, Short-Haul Experimental Engine. NASA TM X-3222, 1975.

3. Hancock, J. P.; and Hinson, B. L.: Inlet Development for the L-500. AIAA Paper 69-448, June 1969.

4. Albers, James A.: Theoretical and Experimental Internal Flow Characteristics of a 13.97-Centimeter-Diameter Inlet at STOL Takeoff and Approach Conditions. NASA TN D-7185, 1973.

5. Felderman, E. John; and Albers, James A.: Comparison of Experimental and Theoretical Boundary-Layer Separation for Inlets at Incidence Angle at Low-Speed Conditions. NASA TM X-3194, 1975.

6. Albers, James A.; and Miller, Brent A.: Effect of Subsonic Inlet Lip Geometry on Predicted Surface and Flow Mach Number Distributions. NASA TN D-7446, 1973.

7. Albers, James A.; and Felderman, E. John: Boundary-Layer Analysis of Subsonic Inlet Diffuser Geometries for Engine Nacelles. NASA TN D-7520, 1974.

8. Albers, James A.; Stockman, Norbert O.; and Hirn, John J.: Aerodynamic Analysis of Several High Throat Mach Number Inlets for the Quiet Clean Short-Haul Experimental Engine. NASA TM X-3183, 1975.

9. Boles, M. A.; and Stockman, N. O.: Use of Experimental Separation Limits in the Theoretical Design of V/STOL Inlets. AIAA Paper 77-878, July 1977.

10. Stockman, Norbert O.: Potential and Viscous Flow in VTOL, STOL, or CTOL Propulsion System Inlets. AIAA Paper 75-1186, Oct. 1975.

TABLE I. - FIXED VTOL INLET GEOMETRIC PARAMETERS

Diffuser:	
Diameter of exit, D_e (cm)	30.48
Ratio of length to exit diameter, L_d/D_e	0.55
Ratio of exit flow area to throat area, A_e/A_t	1.066
Ratio of disk exit area to throat area, $A_{e,disk}/A_t$	1.269
Location of inflection point, percent of length	50
Maximum local wall angle, deg	8.7
Equivalent conical half-angle, deg	1.5
Contour of inlet	cubic
Centerbody:	
Ratio of hub to tip diameters, D_c/D_e	0.4
Ratio of major to minor axis	2.0
Contour	ellipse

TABLE II. - VARIED VTOL INLET GEOMETRIC PARAMETERS

Internal lip		External forebody			Overall		
Contraction ratio, $(D_h/D_t)^2$	Ratio of major axis to minor axis	Drag divergence Mach number, M_{dd}	Ratio of maximum to tip diameter, D_{max}/D_e	Ratio of external forebody length to maximum diameter, $\bar{x}/D_{max}$	Ratio of length to diameter, L/D_e	Ratio of length to maximum diameter, L/D_{max}	Ratio of reference surface distance to tip diameter, S_{ref}/D_e
1.46	2.0	0.72	1.156	0.125	0.735	0.928	0.777
		.77	1.185	.193	.735	.905	.777
		.82	1.220	.303	.735	.879	.777
1.65	2.0	0.72	1.226	0.160	0.803	0.901	0.859
		.77	1.305	.240	.803	.874	.859
		.82	1.364	.377	.803	.836	.859
	1.5	.77	1.305	.240	.739	.874	.804
2.2	2.0	0.77	1.642	0.345	0.979	0.802	1.073
2.8	2.0	0.72	1.864	0.285	1.148	0.797	1.277
		.77	1.962	.405	1.148	.757	1.277
		.82	2.101	.608	1.148	.707	1.277

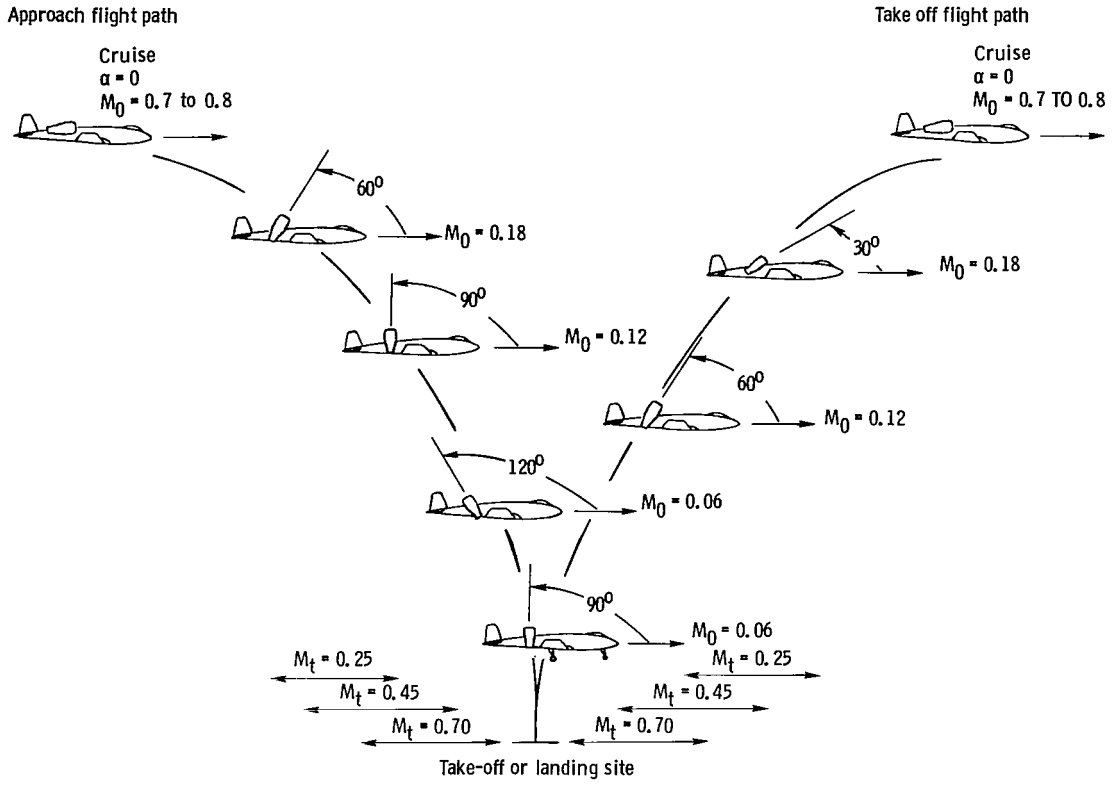

Figure 1. - Representative flight conditions for tilt-nacelle VTOL aircraft.

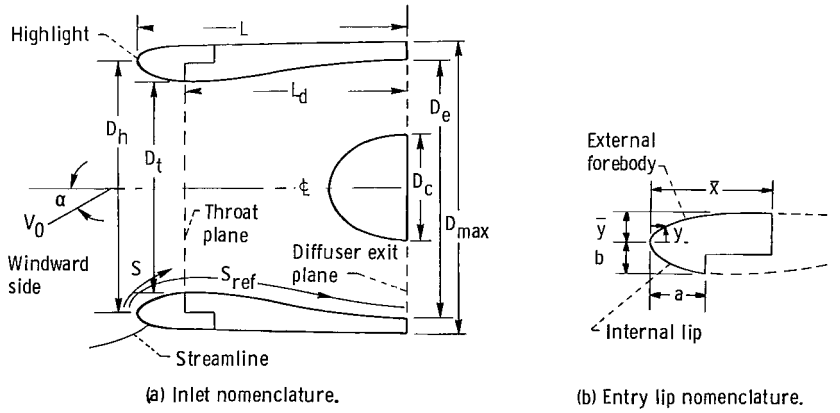

(a) Inlet nomenclature.

(b) Entry lip nomenclature.

Figure 2. - Inlet nomenclature for VTOL inlets.

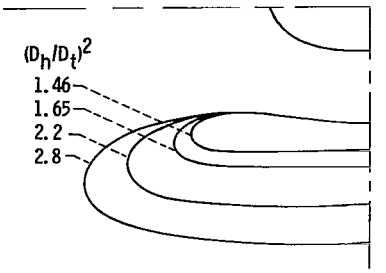

(a) Effect of contraction ratio, $(D_h/D_t)^2$; a/b = 2.0; M_{dd} = 0.77.

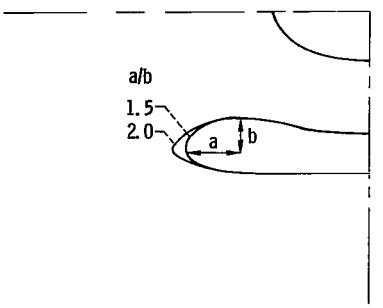

(b) Effect of major-to-minor axis ratio, a/b; $(D_h/D_t)^2$ = 1.65; M_{dd} = 0.77.

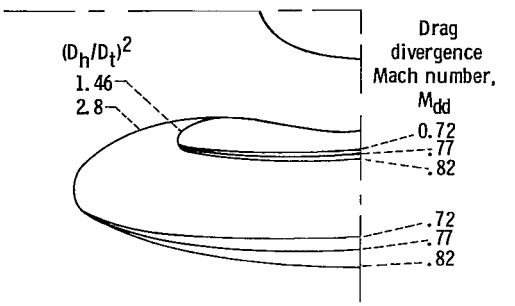

(c) Effect of drag divergence Mach number, M_{dd}, for two contraction ratios; a/b = 2.0.

Figure 3. - Comparison of VTOL inlet geometries.

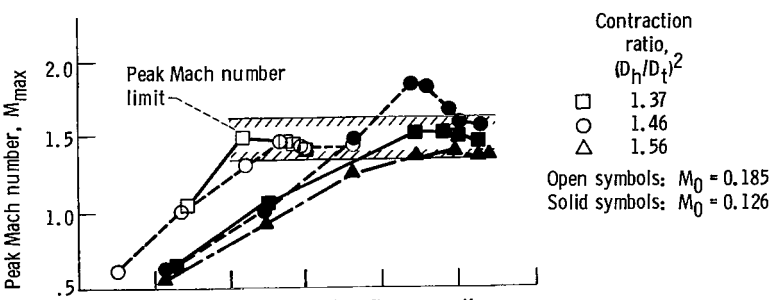

(a) Peak Mach number before flow separation.

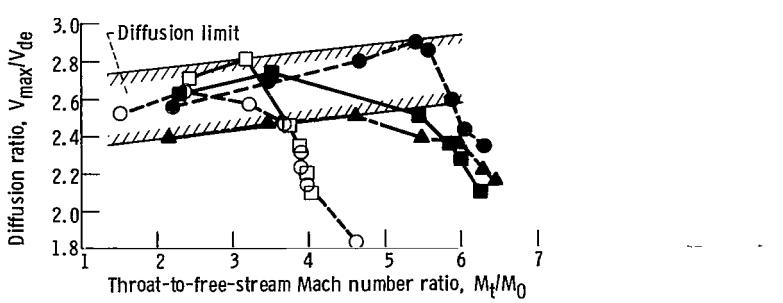

(b) Diffusion ratio before flow separation.

Figure 4. - Experimental separation data for STOL inlets (from ref. 9).

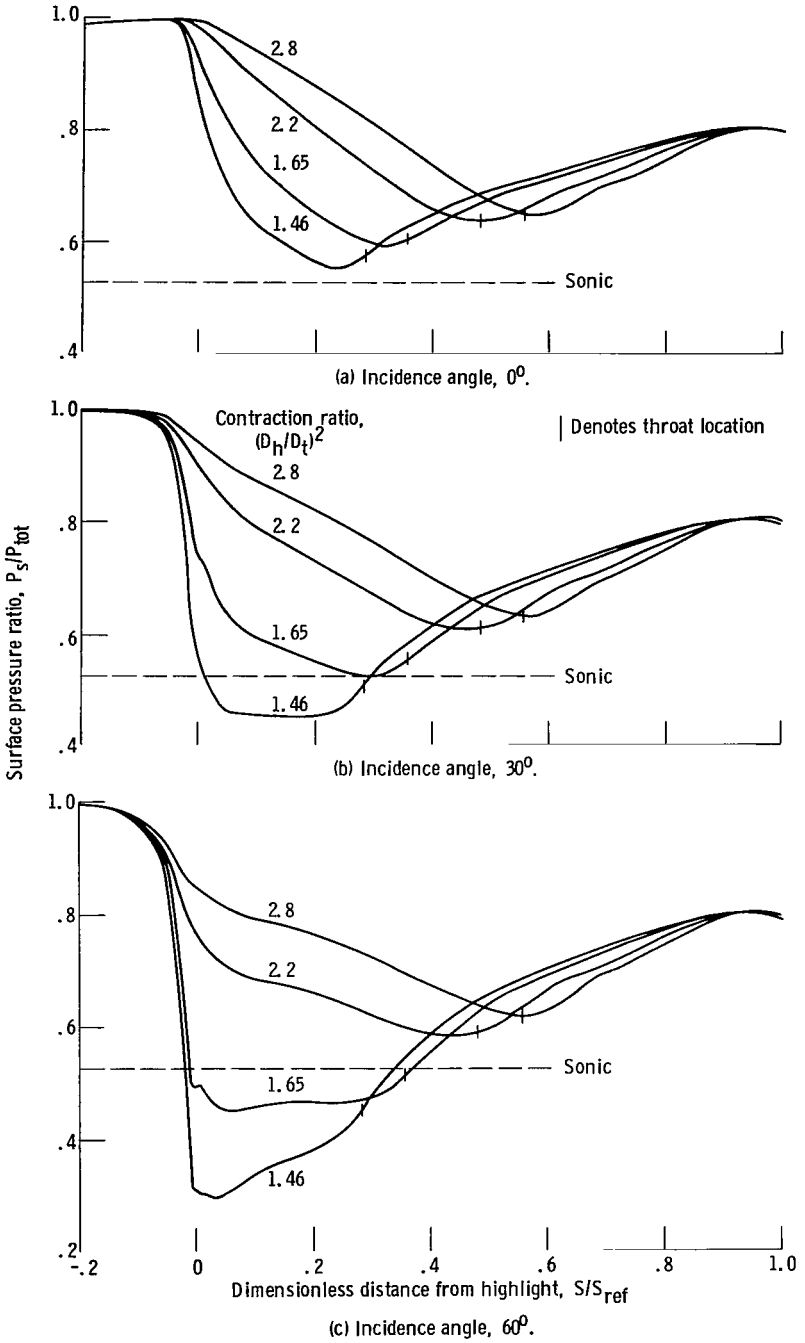

Figure 5. - Theoretical surface pressure ratio distributions for several contraction ratios. $M_t = 0.7$; $M_0 = 0.12$; $M_{dd} = 0.77$; a/b = 2.0.

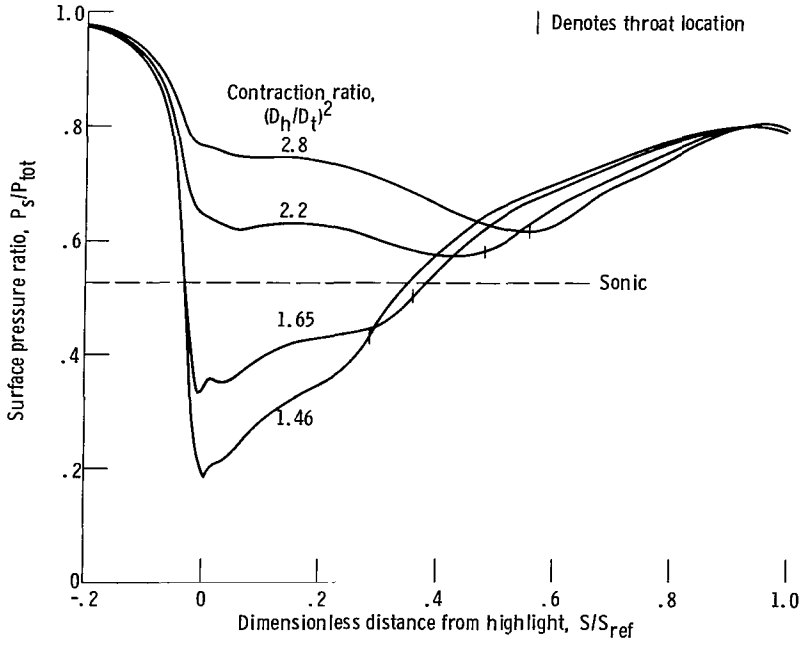

(d) Incidence angle, 90^0.

Figure 5. - Concluded.

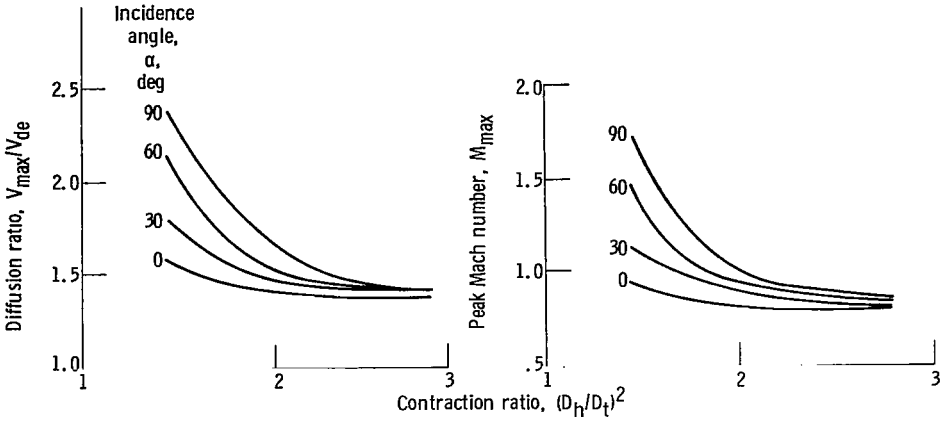

Figure 6. - Effect of contraction ratio on diffusion ratio and peak Mach number. $M_t = 0.7$; $M_0 = 0.12$; $M_{dd} = 0.77$; a/b = 2.0.

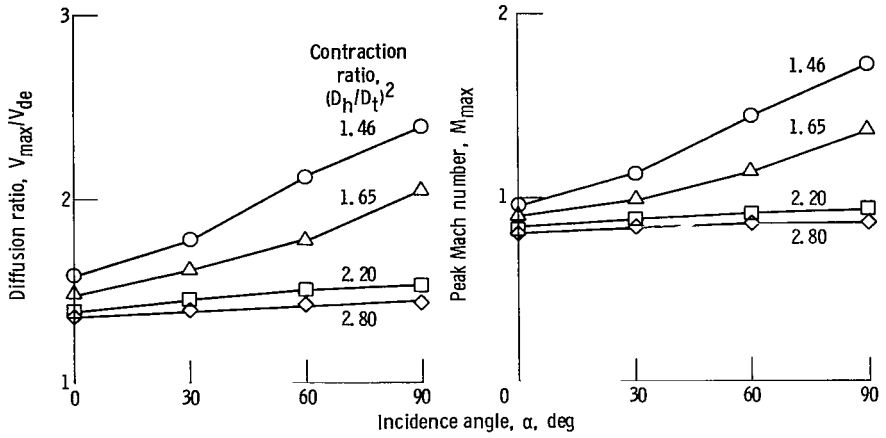

Figure 7. - Effect of incidence angle on diffusion ratio and peak Mach number. $M_t = 0.7$; $M_0 = 0.12$; $M_{dd} = 0.77$; a/b = 2.0.

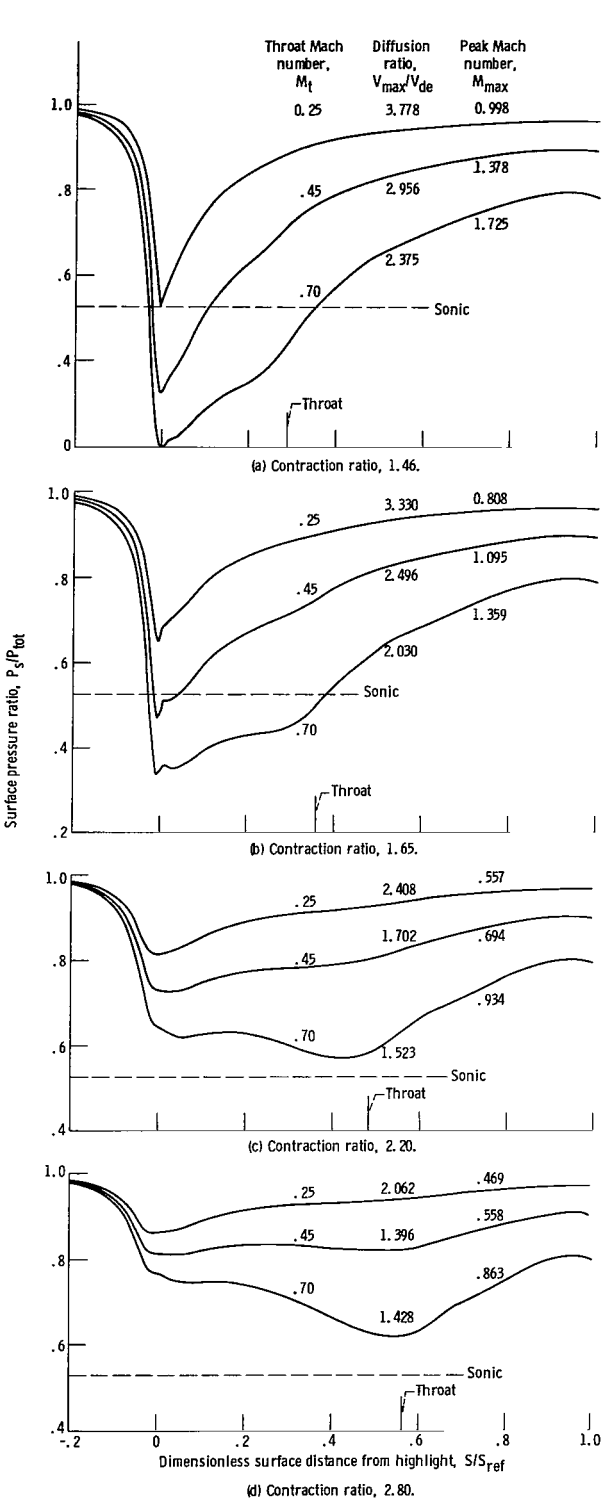

Figure 8. - Theoretical surface pressure distribution at free-stream Mach number of 0.12. $\alpha = 90^0$; $M_{dd} = 0.77$; a/b = 2.0.

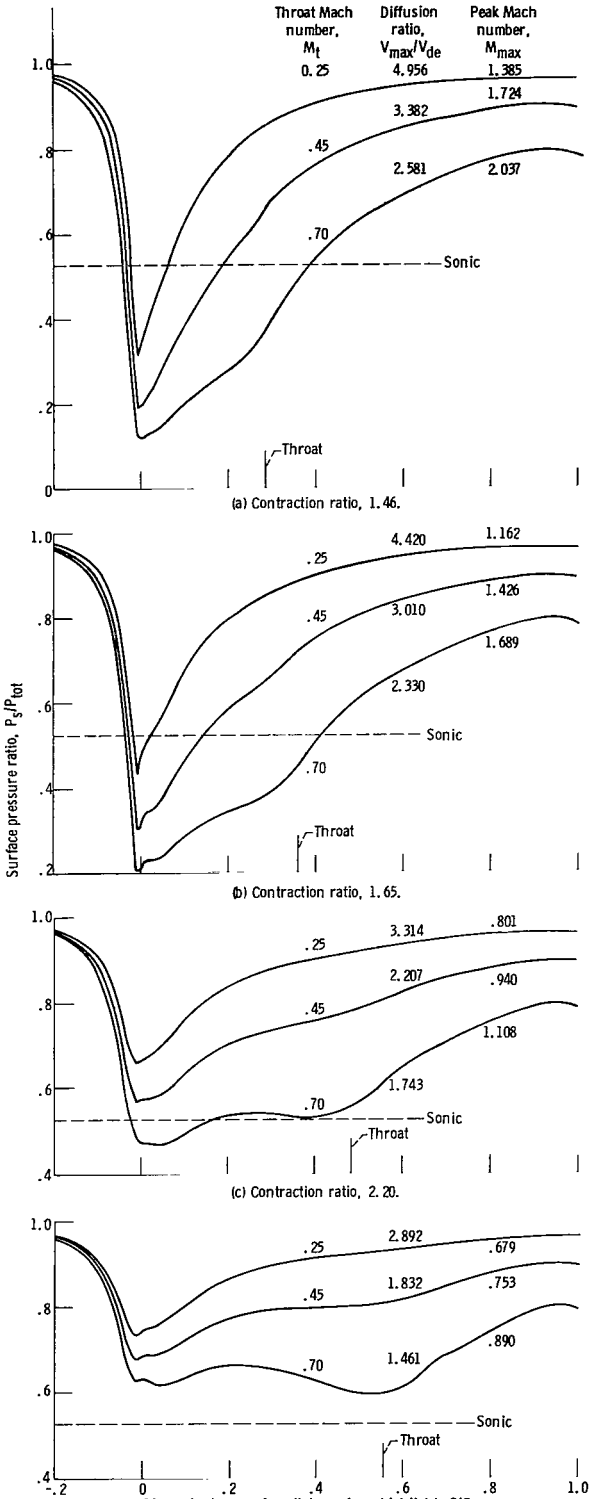

Figure 9. - Theoretical pressure distribution for free-stream Mach number of 0.18. $\alpha = 90^0$; $M_{dd} = 0.77$; a/b = 2.0.

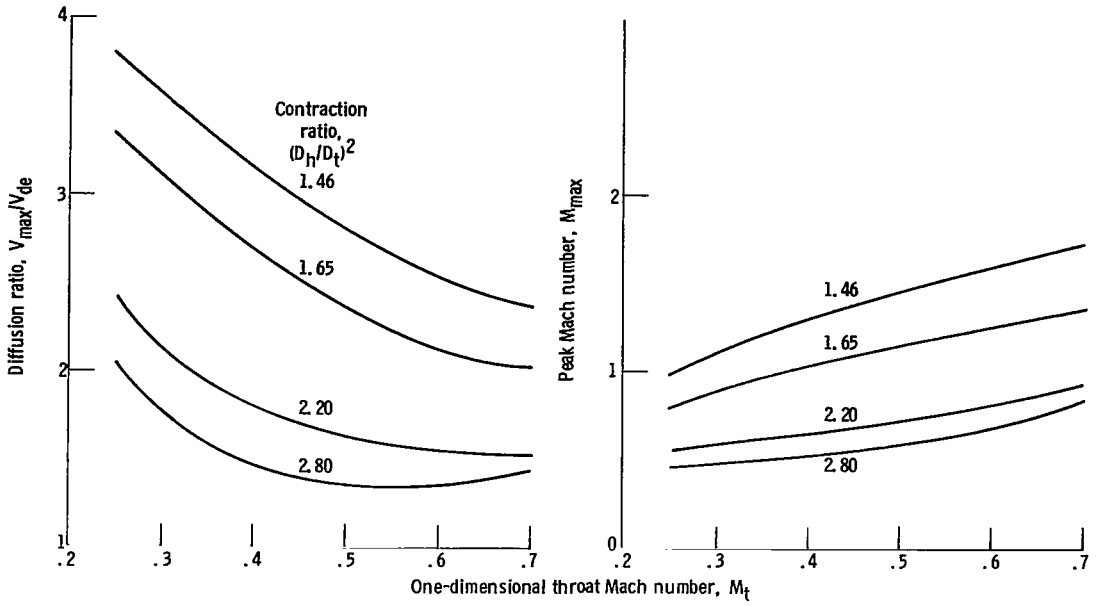

Figure 10. - Effect of one-dimensional throat Mach number on diffusion ratio and peak Mach number at free-stream Mach number of 0.12. $\alpha = 90^0$; $M_{dd} = 0.77$; a/b = 2.0.

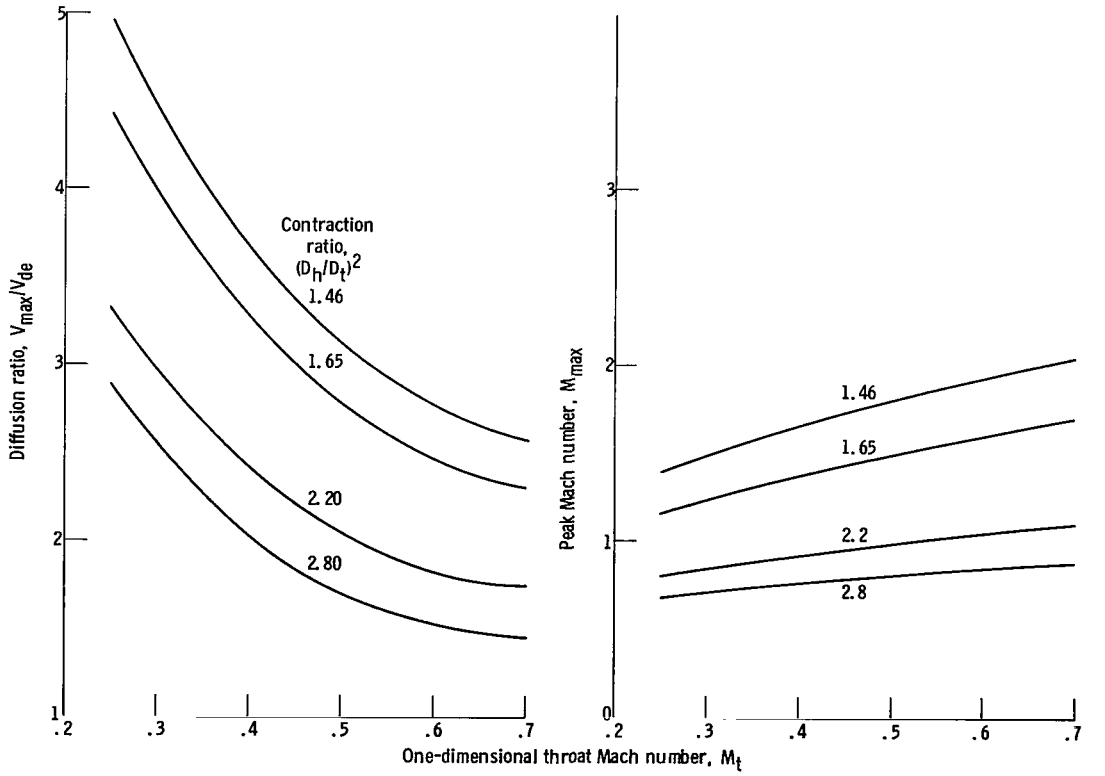

Figure 11. - Effect of one-dimensional throat Mach number on diffusion ratio and peak Mach number at free-stream Mach number of 0.18. $\alpha = 90^0$; $M_{dd} = 0.77$; a/b = 2.0.

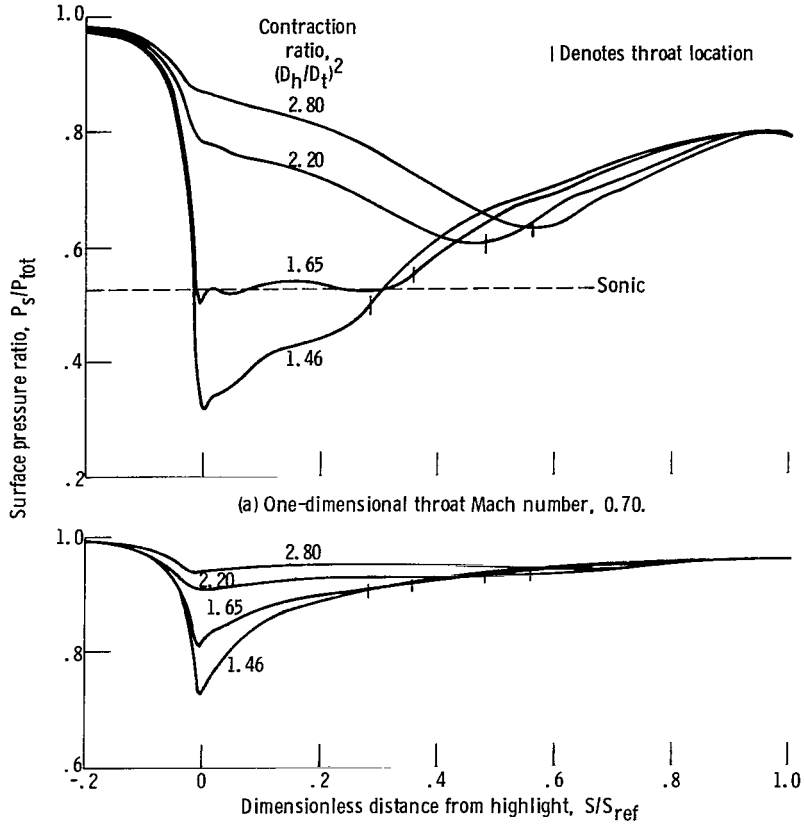

Figure 12. - Effect of contraction ratio on surface static pressure distribution. $\alpha = 120^0$; $M_0 = 0.06$; $M_{dd} = 0.77$; a/b = 2.0.

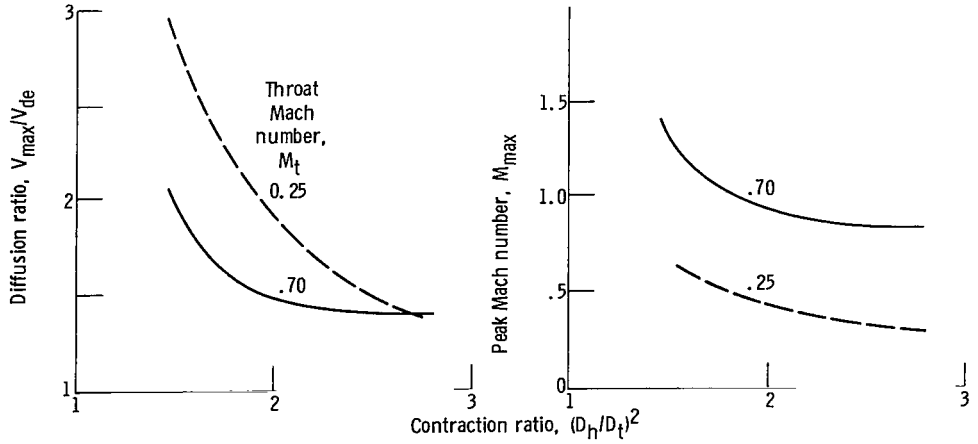

Figure 13. - Effect of contraction ratio on diffusion ratio and peak Mach number. $\alpha = 120^0$; $M_0 = 0.06$; $M_{dd} = 0.77$; a/b = 2.0.

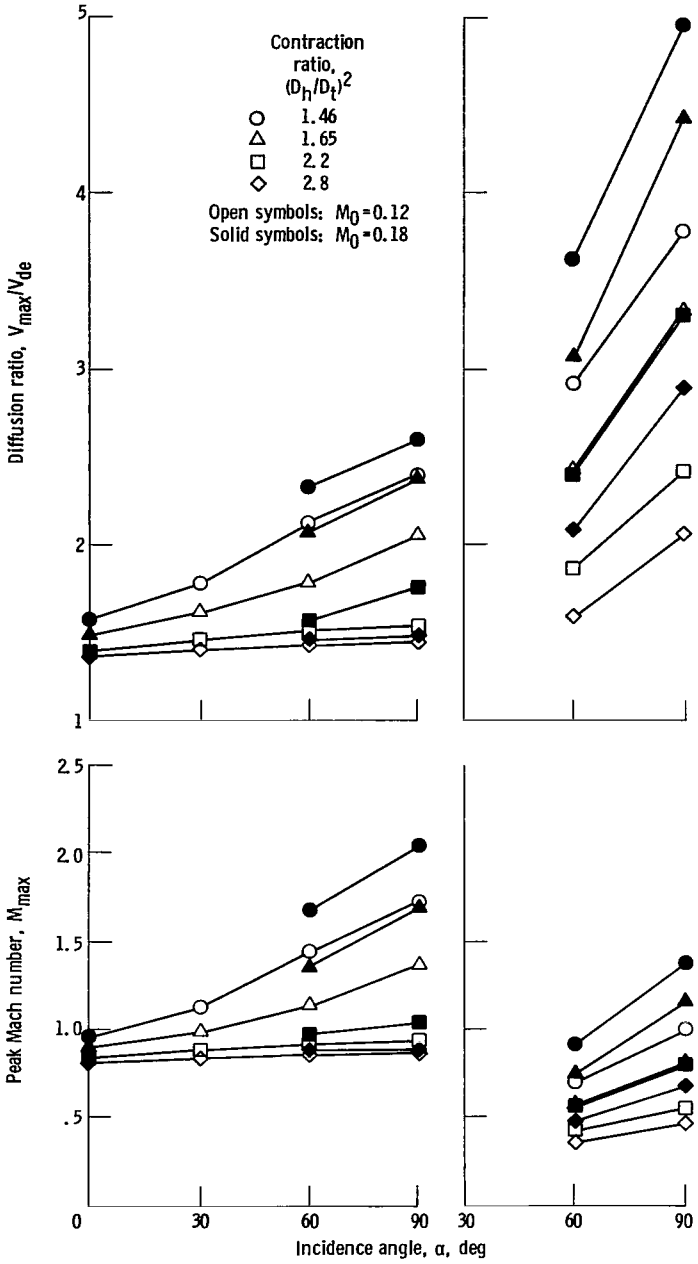

(a) One-dimensional throat Mach number, 0.70.

(b) One-dimensional throat Mach number, 0.25.

Figure 14. - Summary of the effect of contraction ratio on variation of diffusion ratio and peak Mach number with incidence angle. M_{dd} = 0.77; a/b = 2.0.

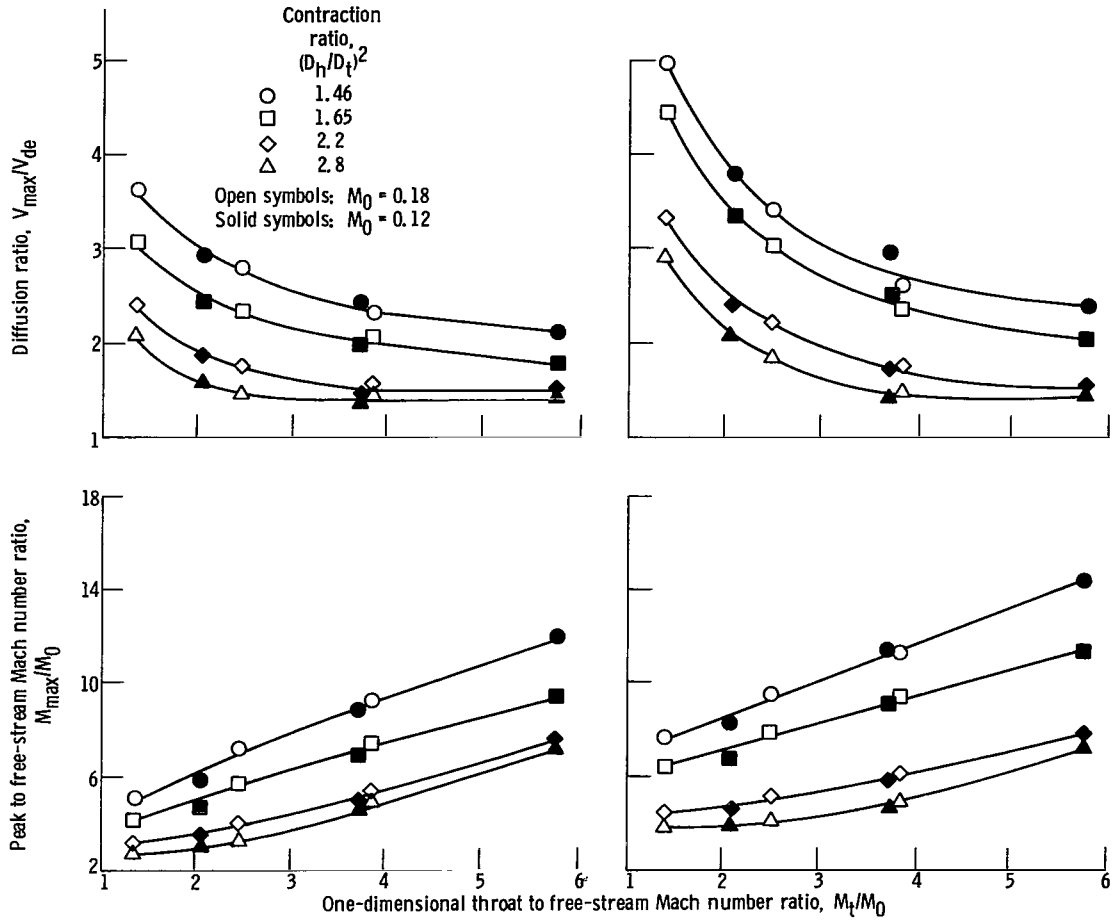

(a) Incidence angle, 60°. (b) Incidence angle, 90°.

Figure 15. - Effect of contraction ratio on diffusion ratio and peak Mach number as functions of one-dimensional throat to free-stream Mach number ratio. M_0 = 0.12 and 0.18; M_{dd} = 0.77; a/b of 2.0.

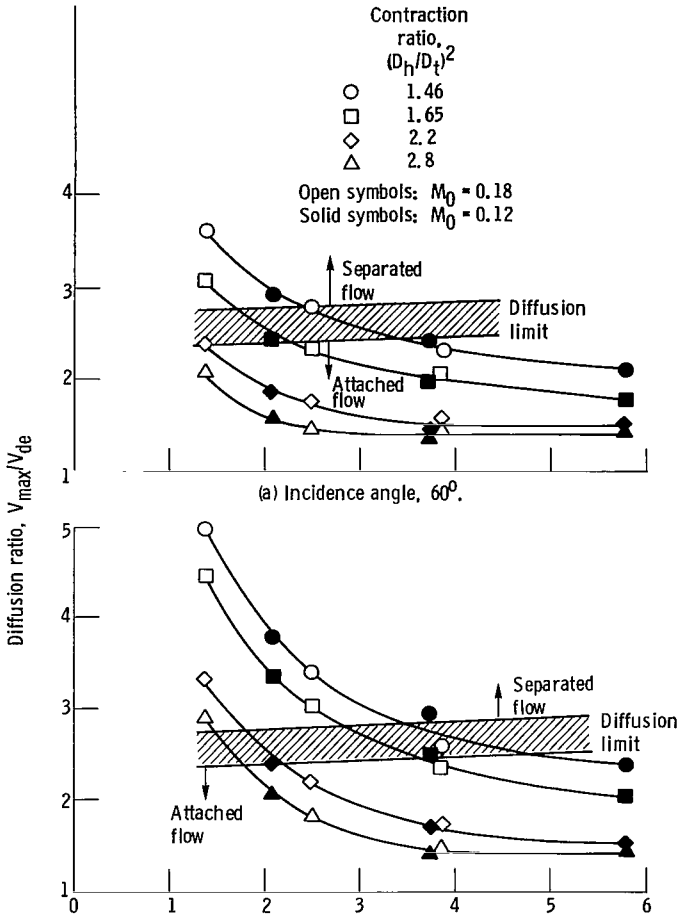

Figure 16. - Theoretical VTOL diffusion ratio with experimental STOL separation limits versus one-dimensional-throat to free-stream Mach number ratio. $M_{dd} = 0.77$; $a/b = 2.0$.

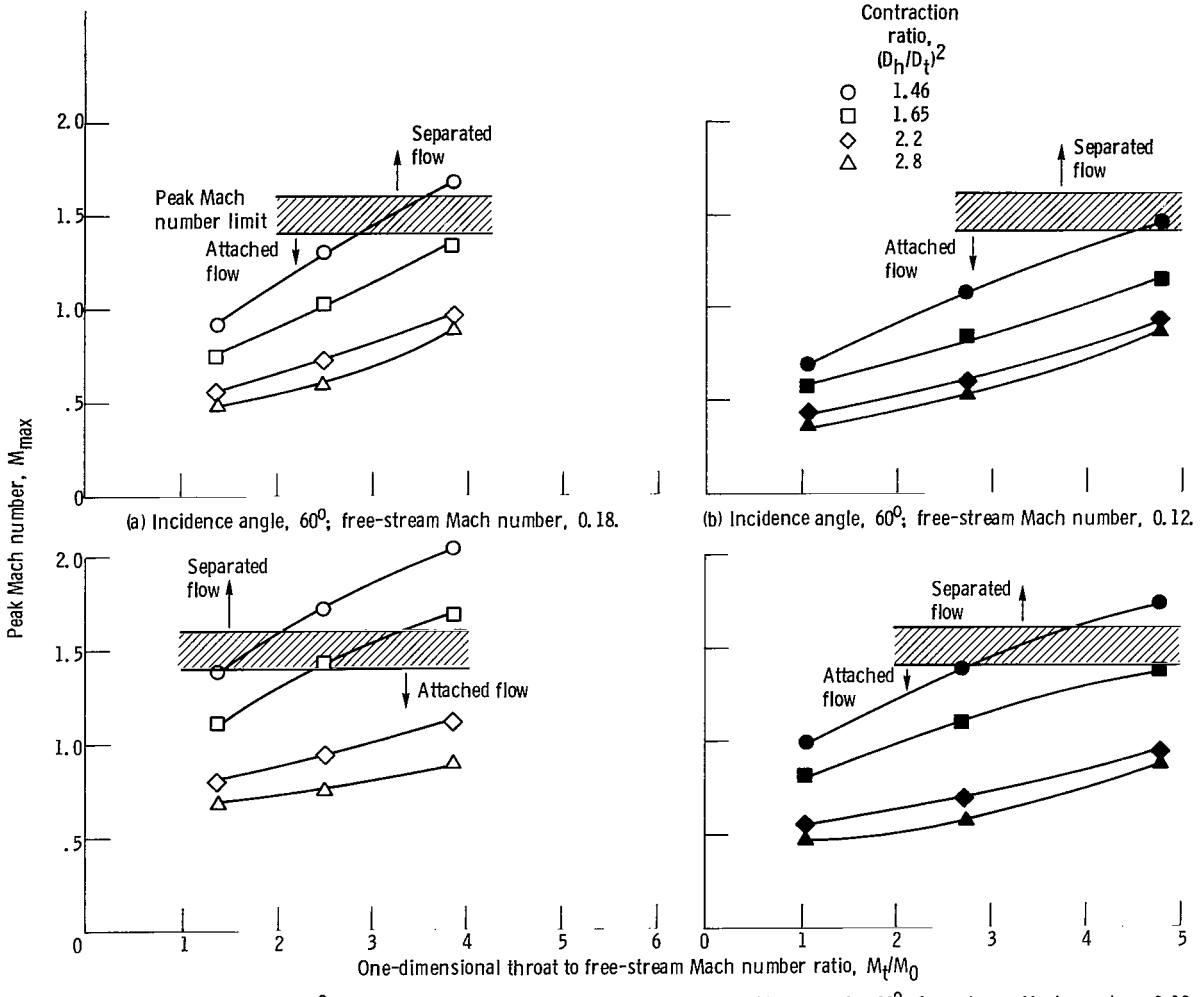

Figure 17. - Theoretical VTOL peak Mach number with experimental STOL separation limits versus one-dimensional throat-to free-stream Mach number ratio. $M_{dd} = 0.77$; $a/b = 2.0$.

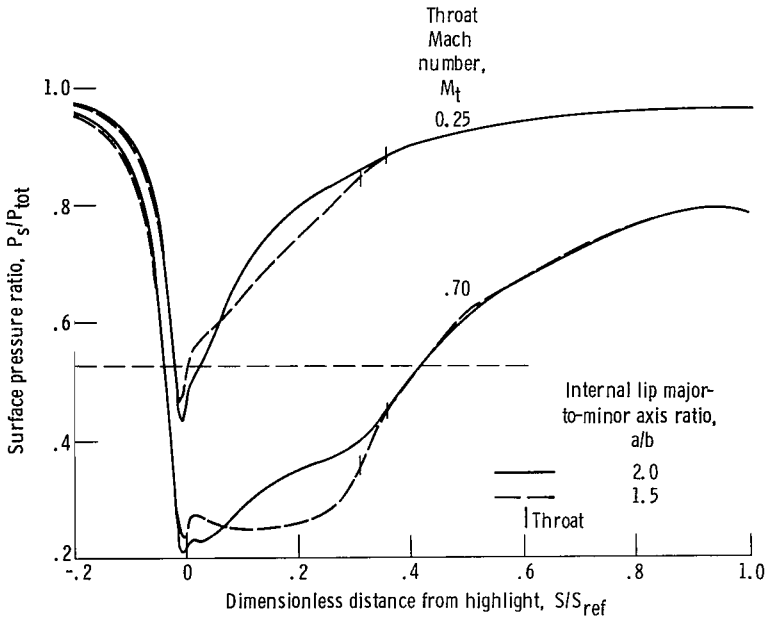

Figure 18. - Effect of major-to-minor axis ratio on surface pressure ratio. $\alpha = 90^0$; $M_0 = 0.18$; $(D_h/D_t)^2 = 1.65$; $M_{dd} = 0.77$.

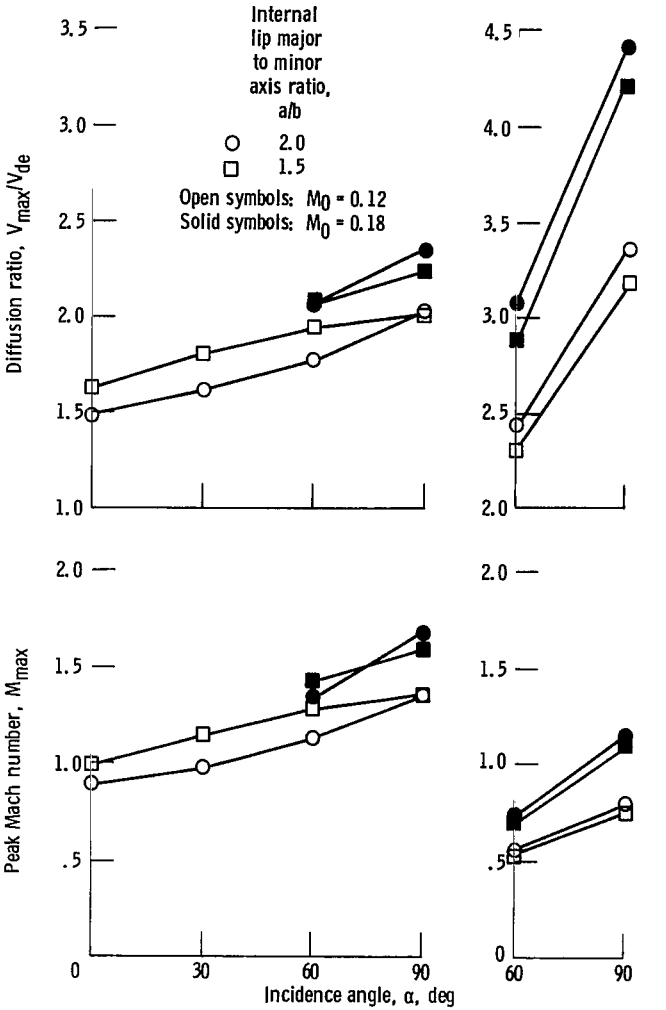

(a) One-dimensional throat Mach number, 0.70.

(b) One-dimensional throat Mach number, 0.25.

Figure 19. - Effect of incidence angle on diffusion ratio and peak Mach number for major-to-minor axis ratio variation. $(D_h/D_t)^2 = 1.65$; $M_{dd} = 0.77$.

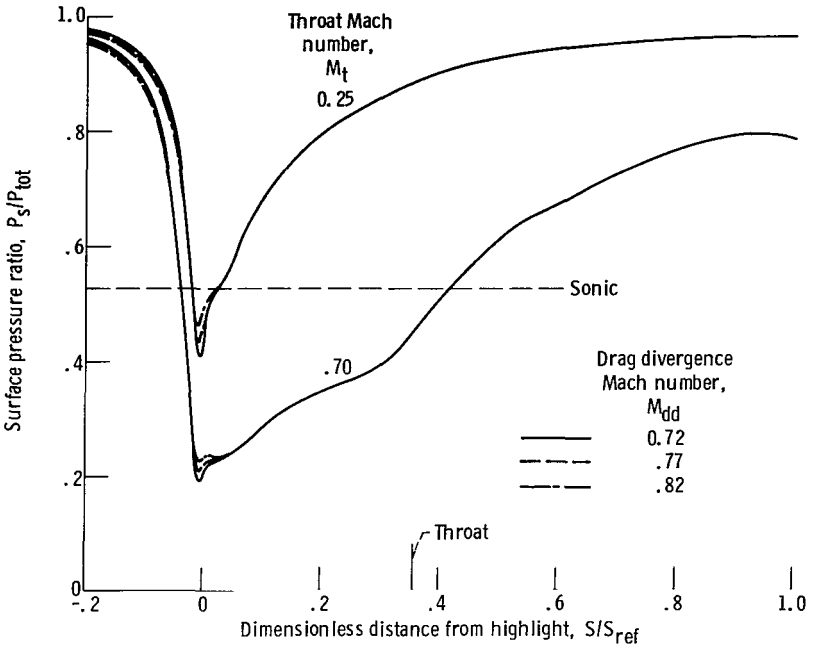

Figure 20. - Effect of drag divergence Mach number on surface pressure ratio. $\alpha = 90^0$; $M_0 = 0.18$; $(D_h/D_t)^2 = 1.65$; a/b = 2.0.

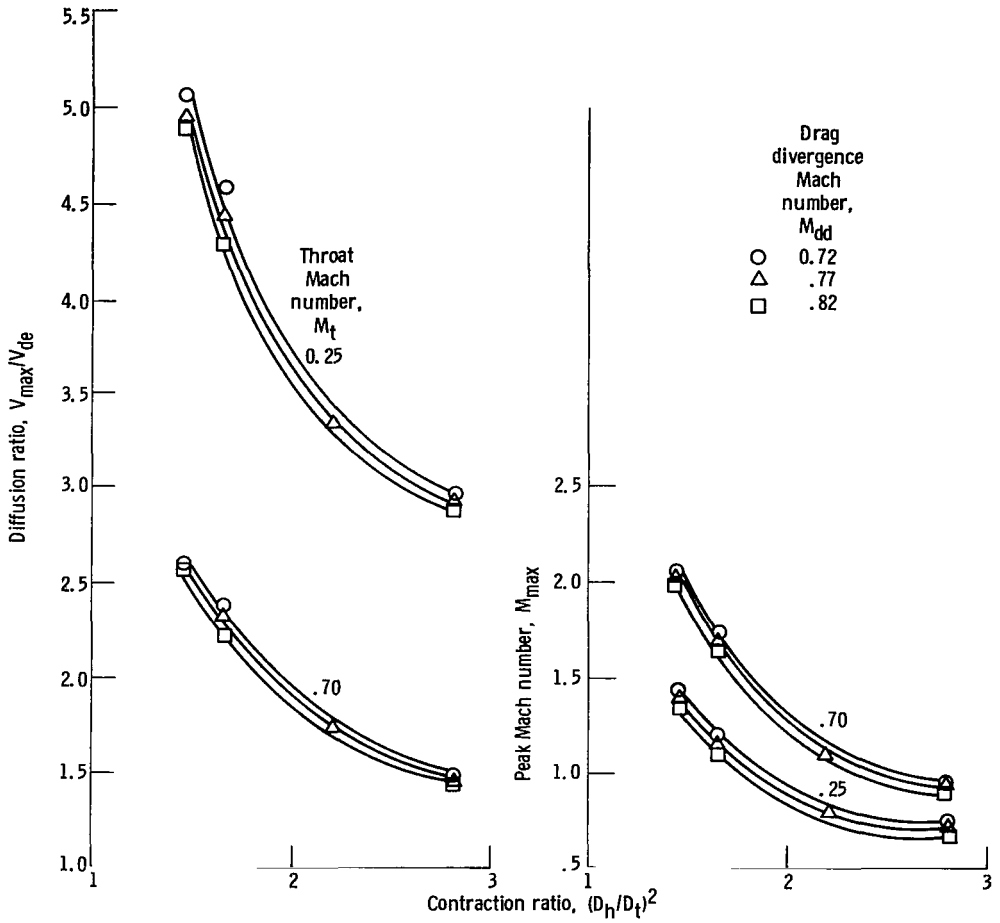

Figure 21. - Effect of drag divergence Mach number on diffusion ratio and peak Mach number for contraction ratio variation. $\alpha = 90^0$; $M_0 = 0.18$; $(D_h/D_t)^2 = 1.65$; $a/b = 2.0$.

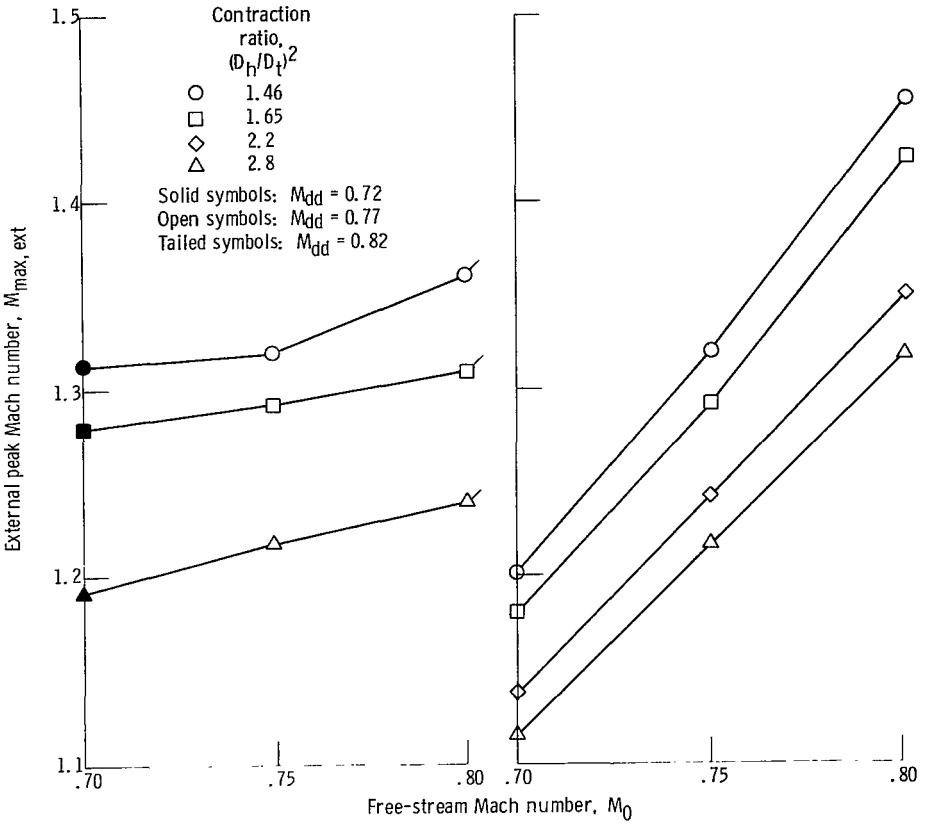

(a) Design cruise Mach number. (b) Off-design cruise Mach number.

Figure 22. - Effect of nacelle geometry on external peak Mach number for cruise. $\alpha = 0$; $M_t = 0.70$; a/b = 2.0.

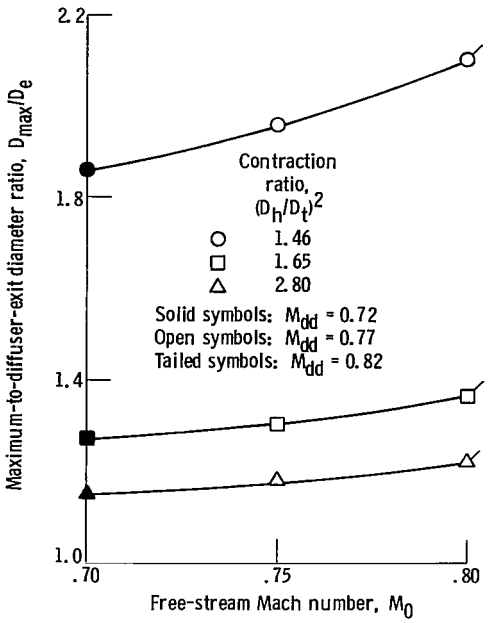

Figure 23. - Effect of contraction ratio and drag divergence Mach number on maximum-to-diffuser exit diameter ratio.

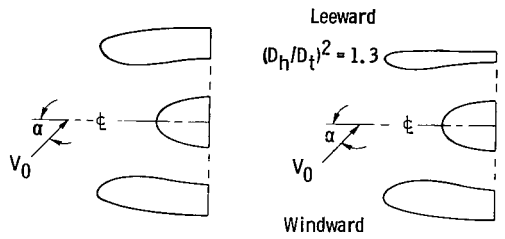

(a) Symmetric inlet. (b) Asymmetric inlet.

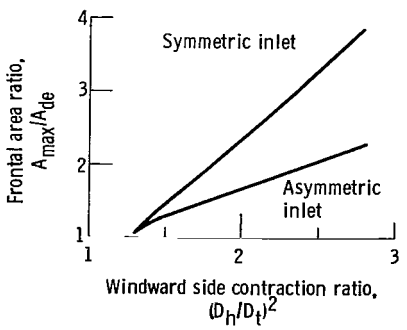

(c) Frontal area ratio.

Figure 24. - Comparison of symmetric and assymetric inlet geometries.

1. Report No.	2. Government Accession No.	3. Recipient's Catalog No.
NASA TP-1205		

4. Title and Subtitle
THEORETICAL FLOW CHARACTERISTICS OF INLETS FOR TILTING-NACELLE VTOL AIRCRAFT

5. Report Date
April 1978

6. Performing Organization Code

7. Author(s)
Michael A. Boles, Roger W. Luidens, and Norbert O. Stockman

8. Performing Organization Report No.
E-9387

10. Work Unit No.
505-05

9. Performing Organization Name and Address
National Aeronautics and Space Administration
Lewis Research Center
Cleveland, Ohio 44135

11. Contract or Grant No.

13. Type of Report and Period Covered
Technical Paper

12. Sponsoring Agency Name and Address
National Aeronautics and Space Administration
Washington, D.C. 20546

14. Sponsoring Agency Code

15. Supplementary Notes

16. Abstract
The results of a theoretical investigation of geometric variables for lift-cruise-fan, tilting-nacelle inlets operating at high incidence angles are presented. These geometric variables are investigated for their effects on surface static-to-free-stream-total-pressure ratio, and the separation parameters of maximum-to-diffuser-exit-surface-velocity ratio and maximum surface Mach number for low-speed (takeoff and landing) operating conditions. The geometric parameters varied were the internal-lip contraction ratio, external-forebody-to-diffuser-exit-diameter ratio, external-forebody length-to-diameter ratio (these last two were established by drag-divergence Mach number specification) and internal-lip major-to-minor-axis ratio.

17. Key Words (Suggested by Author(s))
Inlet flow
VTOL

18. Distribution Statement
Unclassified - unlimited
STAR Category 07

19. Security Classif. (of this report)	20. Security Classif. (of this page)	21. No. of Pages	22. Price*
Unclassified	Unclassified	30	A03

* For sale by the National Technical Information Service, Springfield, Virginia 22161

NASA-Langley, 1978

6 1 1U,A, 040878 S00903DS
DEPT OF THE AIR FORCE
AF WEAPONS LABORATORY
ATTN: TECHNICAL LIBRARY (SUL)
KIRTLAND AFB NM 87117

S